

# An integrated Sachs-Wolfe effect vs redshift test for the cosmological parameters

R. Kantowski,<sup>1,\*</sup> B. Chen,<sup>2,†</sup> and X. Dai<sup>1,‡</sup>

<sup>1</sup>*Homer L. Dodge Department of Physics and Astronomy,  
University of Oklahoma, 440 West Brooks, Norman, OK 73019, USA*

<sup>2</sup>*Research Computing Center, Department of Scientific Computing,  
Florida State University, Tallahassee, FL 32306, USA*

(Dated: December 7, 2024)

# Abstract

We describe a method using the integrated Sachs-Wolfe (ISW) effect caused by individual inhomogeneities to determine the cosmological parameters,  $H_0$ ,  $\Omega_m$ , and  $\Omega_\Lambda$ , etc. This ISW-redshift test requires prior knowledge of a standard set of individual density perturbations, i.e., galaxy clusters and/or cosmic voids, including the dynamics of their evolution with redshift  $z$ . It assumes the density perturbations are embedded (equivalently compensated) and makes use of the newly found relation between the ISW temperature perturbation of the CMB and the Fermat potential of the lens. Given measurements of the amplitudes of the temperature variations in the CMB caused by clusters or voids at various redshifts and estimates of their angular sizes or masses, one can constrain the cosmological parameters. If the evolution of the cluster or void densities are not known but the background cosmology is, then this test can be used to constrain their evolution.

PACS numbers: 98.62.Sb, 98.65.Dx, 98.80.-k

Keywords: General Relativity; Cosmology; Gravitational Lensing;

## I. INTRODUCTION

The late time integrated Sachs-Wolfe (ISW) effect [1], also called the Rees-Sciama (RS) effect [2], has recently been suggested (as well and disputed) as the source of observed hot and cold spots in the CMB temperature maps around some known large scale structures—galaxy clusters and cosmic voids [3–5]. By modeling cluster and void density profiles, and by adjusting cluster masses and void depths, observed temperature excesses/deficits can be matched by ISW predictions [6–10]. Several proposals also exist to use lensing of the CMB to determine properties of these clusters and voids as well as the cosmological parameters [11–14]. What we present in this paper is not unrelated to these proposals but offers an easier and more direct method for relating the ISW temperature shifts to the cluster/void structure and the background cosmology. The conventional approach to determine the ISW effect is to first construct the “lensing potential” of a cluster or void from a model of its density profile and then compute the potential’s effect on the observed CMB’s temperature.

---

\* kantowski@ou.edu

† bchen3@fsu.edu

‡ xdai@ou.edu

Our approach uses another lensing quantity, the “Fermat potential” or equivalently the potential part of the time delay, to relate the lens and cosmology to the ISW temperature fluctuations. Our method of evaluating the ISW effect is directly related to the lens’ mass profile and is more transparent than the conventional approach. It is simpler to use and requires the construction of only one single function, the potential part of the time delay [15]. It is also flexible to use, i.e., the lens structure and/or its evolution can easily be varied and the effects of either are separately discerned.

We have recently developed the embedded lens theory [16–22] which could be called the Swiss cheese lens theory, or at lowest order, the compensated lens theory. The theory originated from the Swiss cheese models of general relativity (GR) [23–25], therefore one can be confident of its gravitational predictions, if GR is indeed the correct theory. An embedded lens (a photon deflector) at redshift  $z_d$  is constructed by first removing a comoving sphere of radius  $\chi_b$  from a homogeneous Friedman-Lemaître-Robertson-Walker (FLRW) cosmology producing a Swiss cheese void, see Fig. 1. The void has a physical radius  $r_d = \chi_b R(t_d)$  at cosmic time  $t_d$  that expands with the radius of the background cosmology  $R(t)$  but has a constant angular radius  $\theta_M$  as seen by an observer, as the observer ages. In the lowest order lensing theory [18] these radii are related (by embedding) to the Schwarzschild radius  $r_s$  of the removed mass by

$$\theta_M = \frac{r_d}{D_d} = \frac{1}{1+z_d} \frac{1}{D_d} \left( \frac{r_s}{\Omega_m} \frac{c^2}{H_0^2} \right)^{1/3}, \quad (1)$$

where  $D_d$  is the angular diameter distance of the void’s center in the standard FLRW cosmology,  $H_0$  the Hubble constant, and  $\Omega_m$  the matter density parameter. We next replace the removed mass with any appropriate spherical density while keeping Einstein’s equations satisfied throughout the Swiss cheese void and on its time-evolving boundary. The logic for embedding is simple, by computing the mean density inside larger and larger spheres centered on a density perturbation, a radius will be reached beyond which the mean density coincides with the FLRW background. The minimum radius at which this takes place can be chosen as  $r_d$ . The simplest such exact Swiss cheese models are constructed by filling the void with Lemaître-Tolman-Bondi (LTB) models [26–28]. Since we are only interested in the lowest order lensing theory, any non-relativistic fluid whose net mass is the same as the removed Swiss cheese void’s mass will suffice. Consequently, models of physical voids must be surrounded by higher density regions and cluster models surrounded by lower density

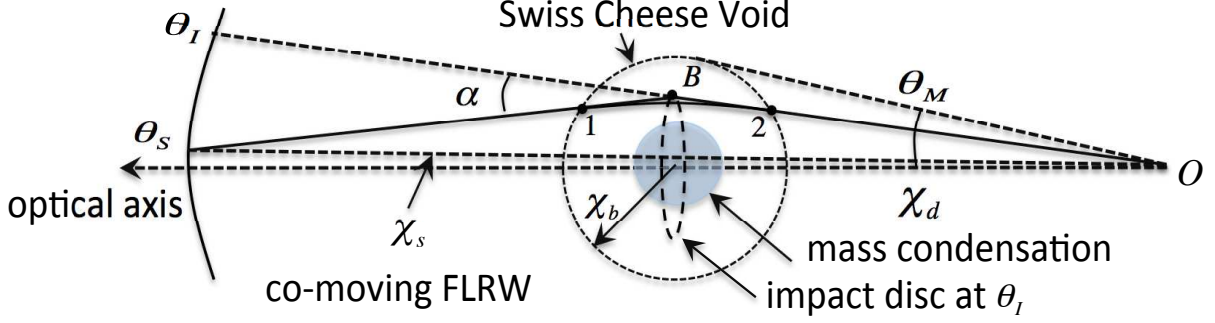


FIG. 1. The comoving geometry of an embedded lens at redshift  $1 + z_d = R_0/R(t_d)$ . Angles  $\theta_S$  and  $\theta_I$  respectively, are source and image angles;  $\chi_d$  and  $\chi_s$  are the comoving angular distances of the lens and the source. The (constant) angular size of the void is  $\theta_M \equiv \chi_b/\chi_d$  in lowest order lensing theory where  $\chi_b$  is the comoving radius of the Swiss cheese void. The physical radius of the deflecting lens depends on the cosmic time  $t_d$ , i.e.,  $r_d = R(t_d)\chi_b$ . The shadowed area represents an embedded cluster. The dashed circle shows the impact disc of angular radius  $\theta_I$ , used to compute the included projected mass fraction  $f(x)$  of the lens, see Eq. (2). The equivalent figure for a void lens has a mass condensation surrounding a low density central region and a repulsive instead of attractive deflection angle  $\alpha$ .

regions. Such linearized gravitational models are often referred to as compensated [29–34].

For spherical density perturbations we have shown in [20, 21] that to lowest order an embedded lens can be completely described by its Fermat potential (equivalent to the sum of the geometrical and potential time delays,  $cT = cT_g + T_p$ )

$$cT(\theta_S, \theta_I) = (1 + z_d) \frac{D_d D_s}{D_{ds}} \left[ \frac{(\theta_S - \theta_I)^2}{2} + \theta_E^2 \int_x^1 \frac{f(x', z_d) - f_{\text{RW}}(x')}{x'} dx' \right]. \quad (2)$$

Here  $x \equiv \theta_I/\theta_M$  is the normalized image angle,  $f(x) \equiv M_{\text{disc}}(\theta_I)/M_{\text{disc}}(\theta_M)$  is the fraction of the embedded lens' mass projected within the impact disc of angular radius  $\theta_I$ , and  $f_{\text{RW}}(x) = 1 - (1 - x^2)^{3/2}$  is the corresponding quantity for the removed co-moving FLRW dust sphere. At (and beyond) the boundary of the embedded lens,  $f(x) = f_{\text{RW}}(x) = 1$ . The angle  $\theta_E = \sqrt{2r_s D_{ds}/D_d D_s}$  is the usual Einstein ring angle. Distances  $D_s$  and  $D_{ds}$  are angular diameter distances to the source measured from the observer and the deflector, respectively. The geometrical part of the time delay  $T_g$ , i.e., the first term in Eq. (2), has a universal form whereas the potential part  $T_p$  depends on the individual lens structure. To

construct the Fermat potential all that is needed is a mass density profile  $\rho(r, z_d)$  for which

$$cT_p(\theta_I, z_d) = 2(1 + z_d)r_s \int_x^1 \frac{f(x', z_d) - f_{\text{RW}}(x')}{x'} dx', \quad (3)$$

can be integrated. All embedded lens properties can be constructed once the specific  $T_p(\theta_I, z_d)$  is known. For example the specific lens equation is given by a  $\theta_I$ -variation  $\delta T(\theta_S, \theta_I)/\delta \theta_I = 0$ . In [21] we have shown that the ISW effect [1, 2] is obtained by a  $z_d$ -derivative of  $T_p$  (or  $T$  since  $\partial T_g/\partial z_d \equiv 0$ )

$$\frac{\Delta \mathcal{T}(\theta_I, z_d)}{\mathcal{T}} = H_d \frac{\partial T_p(\theta_I, z_d)}{\partial z_d}. \quad (4)$$

In this expression  $\Delta \mathcal{T}$  is the change in the CMB's temperature  $\mathcal{T}$  caused by CMB photons passing through an evolving gravitational lens at impact angle  $\theta_I$ . The cosmic-time evolution of the lens is replaced by a dependence on the redshift  $z_d$  at which it is seen and the Hubble parameter at that redshift is denoted by  $H_d = H(z_d)$ . To compute the ISW effect caused by an embedded lens, we need not only the density profile required by conventional lens theory [35] to compute image properties, but we also need the density profile's evolution rate to compute the  $z_d$ -derivative.

## II. THE PRINCIPLE BEHIND THE ISW-Z TEST

Equation (4) gives the fluctuation in the observed CMB temperature as a function of angular position across a given, possibly evolving, density perturbation (a lens) caused by the ISW effect. From Eq. (4) the ISW signal is seen to depend on the lens' redshift  $z_d$ , its mass  $r_s$ , its projected fractional density profile  $f(x, z_d)$  including its evolution with redshift, as well as the background cosmology. We construct the new cosmology test using this simple relation. By splitting Eq. (4) into an amplitude term proportional to the product of the lens mass and the Hubble parameter, times a lens structure dependent term  $\mathcal{S}(\theta_I, z_d)$  we have

$$\frac{\Delta \mathcal{T}(\theta_I, z_d)}{\mathcal{T}} = 2r_s \frac{H_d}{c} \times \mathcal{S}(\theta_I, z_d), \quad (5)$$

where the lens structure dependent term is defined by

$$\mathcal{S}(\theta_I, z_d) \equiv \frac{\partial}{\partial z_d} \left[ (1 + z_d) \int_x^1 \frac{f(x', z_d) - f_{\text{RW}}(x')}{x'} dx' \right]. \quad (6)$$

If the lens mass and structure are known, the amplitude of  $\Delta \mathcal{T}(\theta_I, z_d)/\mathcal{T}$  at the lens' center ( $\theta_I = 0$ ) can in principle be used to determine the Hubble parameter  $H(z_d)$ . In practice

to apply Eq. (5) to a cold or hot spot associated with a single void or cluster lens it must be averaged over the aperture of the detector, i.e.,  $\Delta\mathcal{T}(\theta_I, z_d)$  and  $\mathcal{S}(\theta_I, z_d)$  are replaced by their averaged values,  $\Delta\mathcal{T}(z_d)$  and  $\mathcal{S}(z_d)$ . If a uniform set of clusters and/or voids can be found whose redshifts, masses, and evolving structures can be determined, then  $\mathcal{S}(\theta_I, z_d)$  and  $\mathcal{S}(z_d)$  can be determined. Given the CMB temperature data at the positions of these clusters and/or voids, Eq. (5) will determine the Hubble parameter  $H_d$  as a function of  $z_d$ . The redshift dependent Hubble parameter can then be used to constrain cosmological parameters such as  $H_0$ ,  $\Omega_m$  and  $\Omega_\Lambda$ . In Sec. III we illustrate the procedure by applying it to simply top-hat cluster and void models.

The above form of the ISW-z test assumes the mass of the lensing cluster or void is known; however for cosmic voids, radii can be more easily determined than masses [36]. We now present a second form of the ISW-redshift test preferable for such voids. This second test requires knowledge of the energy content of the FLRW background before it can be applied. We construct this form of ISW-redshift test by looking at the central region of the void or cluster, eliminating  $r_s$  from Eq. (4) by using Eq. (1), and dividing by the cube of the angular radius of the Swiss cheese void  $\theta_M^3$  to obtain the  $H_0$  and  $r_s$  independent result

$$\frac{\Delta\mathcal{T}(z_d)/\mathcal{T}}{(\theta_M)^3} = \mathcal{C}(z_d) \times \mathcal{S}(z_d), \quad (7)$$

where the pure curvature dependent part  $\mathcal{C}(z_d)$  is defined by

$$\mathcal{C}(z_d) \equiv 2\Omega_m \frac{H_d}{H_0} \left[ (1 + z_d) D_d \frac{H_0}{c} \right]^3, \quad (8)$$

and the lens structure dependent term  $\mathcal{S}(z_d)$  is again defined by Eq. (6).

By replacing the Hubble parameter  $H_d$  and the angular diameter distance  $D_d$  by functions of the curvature and redshift, assuming for example a  $\Lambda$ CDM gravity source,

$$H_d/H_0 \equiv E(z_d) = \sqrt{\Omega_\Lambda + \Omega_m(1 + z_d)^3 + (1 - \Omega_m - \Omega_\Lambda)(1 + z_d)^2}, \quad (9)$$

and

$$(1 + z_d) D_d \frac{H_0}{c} = \frac{1}{\sqrt{|1 - \Omega_m - \Omega_\Lambda|}} \text{Sinh} \left[ \sqrt{|1 - \Omega_m - \Omega_\Lambda|} \int_0^{z_d} \frac{dz}{E(z)} \right], \quad (10)$$

where  $\text{Sinh}(x) = \sin(x)$ ,  $x$ , and  $\sinh(x)$  for a closed, flat, or open universe, respectively. The curvature part of Eq. (7) becomes

$$\mathcal{C}(z_d) \equiv 2\Omega_m E(z_d) \left\{ \frac{1}{\sqrt{|1 - \Omega_m - \Omega_\Lambda|}} \text{Sinh} \left[ \sqrt{|1 - \Omega_m - \Omega_\Lambda|} \int_0^{z_d} \frac{dz}{E(z)} \right] \right\}^3, \quad (11)$$

For  $z_d \ll 1$  the curvature term can be approximated as

$$\mathcal{C}(z_d) \approx 2\Omega_m z_d^3 \left[ 1 - \frac{1}{2} \left( 1 + \frac{1}{2}\Omega_m - \Omega_\Lambda \right) z_d + \left( \frac{3}{4} - \frac{1}{4}\Omega_m - \Omega_\Lambda + \frac{1}{16}(\Omega_m - 2\Omega_\Lambda)^2 \right) z_d^2 + \mathcal{O}[z_d^3] \right] \quad (12)$$

We plot the curvature part, Eq. (11), in Fig. 2 for four familiar cosmologies: the Einstein de Sitter (EdS) universe,  $(\Omega_m, \Omega_\Lambda) = (1, 0)$ ; a dark matter only universe,  $(\Omega_m, \Omega_\Lambda) = (0.3, 0)$ ; a  $\Lambda$ CDM universe,  $(\Omega_m, \Omega_\Lambda) = (0.3, 0.7)$ ; and a baryonic matter only universe,  $(\Omega_m, \Omega_\Lambda) = (0.05, 0)$ . Cosmic voids identified through galaxy surveys generally have low redshifts  $z \lesssim 0.5$  [37, 38], and as can be seen in Eq. (12), at small redshifts the curvature term is dominated by the mass density parameter  $\Omega_m$ . Consequently, this test should place strong constraints on  $\Omega_m$ .

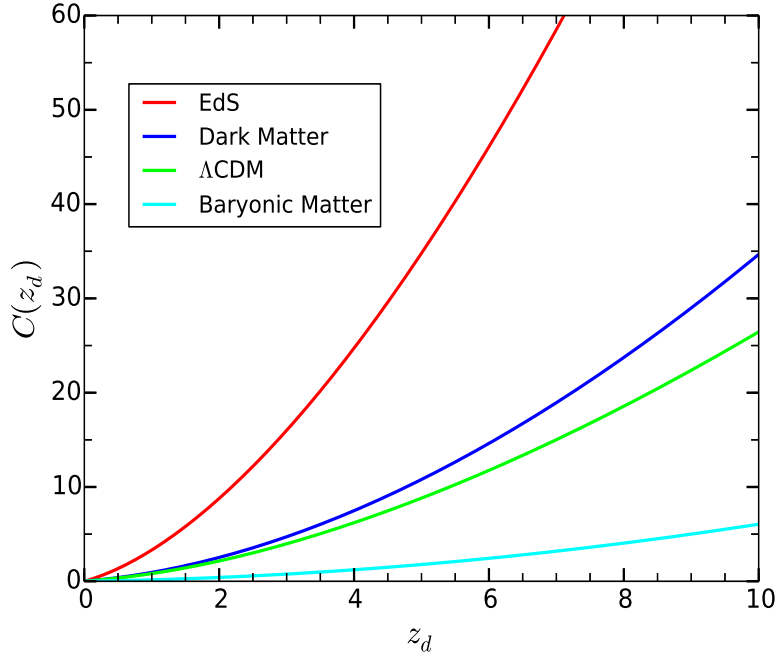


FIG. 2. Redshift dependence of the curvature term  $\mathcal{C}(z_d)$  from Eq. (11) for four background cosmologies (from top to bottom): the Einstein de Sitter universe,  $(\Omega_m, \Omega_\Lambda) = (1, 0)$ , red; a dark matter only universe,  $(\Omega_m, \Omega_\Lambda) = (0.3, 0)$ , blue; a  $\Lambda$ CDM universe,  $(\Omega_m, \Omega_\Lambda) = (0.3, 0.7)$ , green; and a baryonic matter only universe,  $(\Omega_m, \Omega_\Lambda) = (0.05, 0)$ , cyan.  $\mathcal{C}(z_d)$  depends strongly on  $\Omega_m$  but only weakly on  $\Omega_\Lambda$ .

### III. EXAMPLES

The structure term  $\mathcal{S}(\theta_I, z_d)$  has to be properly modeled before we can use either of the two tests presented in the previous section to constrain the cosmological parameters. Modeling strong gravitational lenses (galaxies or clusters of galaxies) traditionally requires only the density profiles  $\rho(\mathbf{r})$  of the lenses, whereas modeling ISW effects requires the additional knowledge of the evolution rates of those lenses. Even if we assume that galaxy clusters are virialized (with constant physical radii), their density contrasts with respect to the FLRW background evolve with redshift, and so do their projected fractional mass profiles  $f(x, z_d)$ . Furthermore to analytically evaluate Fermat potentials for compensated cluster lens models with realistic profiles, e.g., cluster lenses with profiles such as the embedded Navarro-Frenk-White (NFW) profile [39] is challenging. Dark matter density profiles for cosmic voids are currently estimated by stacking and averaging galaxy counts over large numbers of voids. This assumes that luminous matter as tracers of dark matter is not significantly biased and even if correct, far less is known about void evolution than about cluster evolution. There are hints indicating that voids can be deep in the central regions, with  $\delta \lesssim -0.8$  near the void center [36]. If this is indeed the case, then  $\delta$  might be evolving very slowly (already approaching its lower bound of  $-1$ ) and the  $z_d$  dependence in  $f(x, z_d)$  can be neglected. If so the structure term would consequently be easier to model. Voids would simply be expanding with the background and the ISW effect would be determined by the time-delay contribution alone [21]. The ISW-z test might be more fruitfully applied to cosmic voids because CMB measurements are contaminated by hot gas emissions from galaxy clusters (especially toward the centers of the clusters) and other secondary anisotropies such as Sunyaev-Zeldovich (SZ) effect [40, 41].

As a first attempt to illustrate the procedure of constructing the structure term  $\mathcal{S}(z_d)$ , we approximate cosmic density perturbations by a two-parameter family of either top-hat models for clusters or inverted top-hat models for voids, see Fig.3. Both the cluster and void models are compensated with density profiles defined as

$$\frac{\rho - \bar{\rho}}{\bar{\rho}} = \begin{cases} \delta & , 0 \leq x < \mathbf{a}, \\ -\delta/(\mathbf{a}^{-3} - 1) & , \mathbf{a} \leq x < 1, \end{cases} \quad (13)$$

where  $\bar{\rho}$  is the cosmic mean at the lens redshift, the parameter  $\mathbf{a}$  delineates the over and under-dense regions, and  $-1 \leq \delta \leq (\mathbf{a}^{-3} - 1)$  is the density contrast of the inner region.



When  $\delta$  is negative this is a void model and when positive a model for an over-density. The density contrast of the outer region ( $a < x \leq 1$ ) is entirely determined by the necessity of compensating for the excess/depleted central density. For this simple top-hat lens model we find

$$\int_0^1 \frac{f(x', z_d) - f_{\text{RW}}(x')}{x'} dx' = -\delta \frac{\log a}{(a^{-3} - 1)}, \quad (14)$$

and the structure term from Eq. (6) is

$$\mathcal{S}(z_d) = -\frac{\delta \log a}{(a^{-3} - 1)} - (1 + z_d) \frac{d\delta}{dz_d} \frac{\log a}{(a^{-3} - 1)} - \frac{(1 + z_d)\delta}{a(a^{-3} - 1)} \frac{da}{dz_d} \left[ 1 + \frac{3 \log a}{a^3(a^{-3} - 1)} \right]. \quad (15)$$

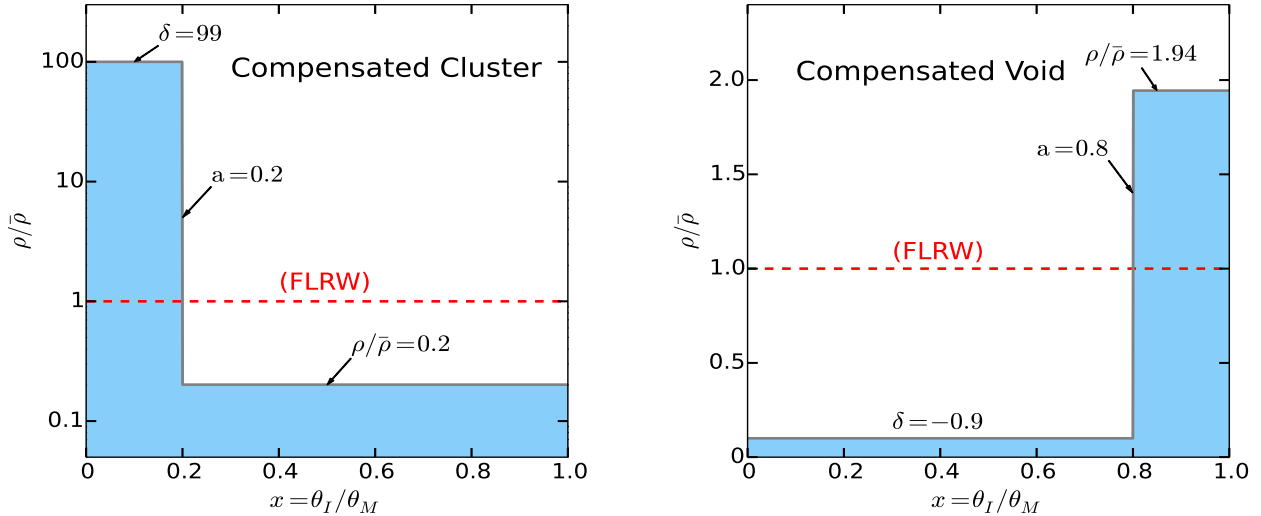


FIG. 3. Compensated top-hat models for a cluster on the left  $a = 0.2, \delta = 99$  and a void on the right  $a = 0.8, \delta = -0.9$ . The well surrounding the cluster (and the wall surrounding the void) begins at physical radius  $r = a r_d$ .

If the lens does not evolve in co-moving space, i.e., if  $\delta$  and  $a$  are both constants, the density perturbation is not evolving in size or shape relative to the background cosmology and  $\mathcal{S}(z_d)$  is just a constant given by Eq. (14). We refer to this non-evolving value as  $S_0$ , see the horizontal dashed brown curve in Fig. 4. If the density perturbation evolves relative to the FLRW background then  $\delta$  and/or  $a$  are functions of the deflector's redshift  $z_d$ , the quantity given by Eq. (14) evolves with time, and the additional derivative terms in Eq. (15) are present. The structure term  $\mathcal{S}(z_d)$  will depend on the background cosmological

parameters if either of the two parameters  $\delta$  or  $\mathbf{a}$  does. If  $\delta$  evolves but  $\mathbf{a}$  does not the second term is present and the perturbation's amplitude evolves relative to the background cosmology but the perturbation doesn't change its shape. Linear perturbations are of this type (see the four cosmological parameter dependent curves in Fig. 4). If  $\mathbf{a}$  evolves the last term is present and the shape of the perturbation evolves. Relaxed clusters (see Fig. 5) and voids produced by explosive motion are of this type [42–44]. We next discuss linear perturbations and relaxed clusters in detail.

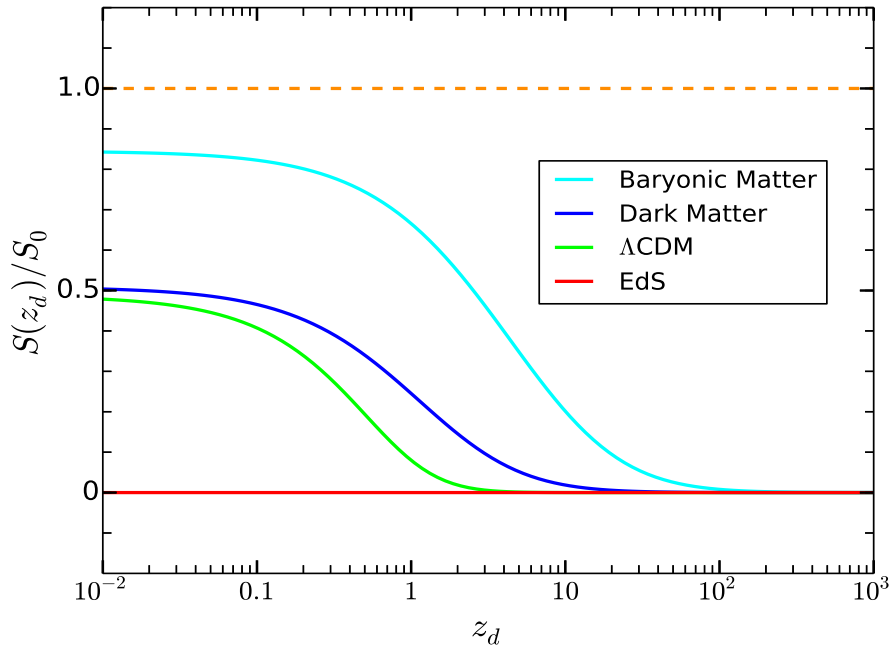


FIG. 4. Redshift evolution of the structure function  $\mathcal{S}(z_d)/\mathcal{S}_0$  where  $\mathcal{S}_0 \equiv -\delta_0 \log \mathbf{a}_0/(\mathbf{a}_0^{-3} - 1)$  for cluster ( $\mathcal{S}_0 > 0$ ) and void ( $\mathcal{S}_0 < 0$ ) models, see Eq. (13). The dashed brown curve is for cluster or void lenses co-expanding with the background cosmology. The solid curves are computed assuming linear evolution in four background cosmologies (bottom to top): the Einstein de Sitter universe,  $(\Omega_m, \Omega_\Lambda) = (1, 0)$ , red; a  $\Lambda$ CDM universe,  $(\Omega_m, \Omega_\Lambda) = (0.3, 0.7)$ , green; a dark matter only universe,  $(\Omega_m, \Omega_\Lambda) = (0.3, 0)$ , blue; and a baryonic-matter only universe,  $(\Omega_m, \Omega_\Lambda) = (0.05, 0)$ , cyan.

### A. Linearly Evolving Cosmic Voids and Large Scale Overdensities

As a first example of the ISW-z test using Eq. (7) we assume linear growth for the clusters or voids of the form given in Eq. (13). The fractional comoving radius of the top-hat remains constant ( $\mathbf{a} = \mathbf{a}_0$ ) while  $\delta$  evolves as

$$\delta = D_+(z_d) \delta_0, \quad (16)$$

where the linear perturbation growth factor [45]

$$D_+(z) = E(z) \int_z^\infty \frac{(1+z')}{[E(z')]^3} dz' \bigg/ \int_0^\infty \frac{(1+z')}{[E(z')]^3} dz', \quad (17)$$

depends on the cosmological parameters through  $E(z)$ , see Eq. (9). Consequently, linear evolution produces an evolving structure dependent term  $\mathcal{S}(z_d)$  that depends on cosmological parameters such as  $\Omega_m$  and  $\Omega_\Lambda$ ,

$$\mathcal{S}(z_d) = -\delta_0 \frac{\log \mathbf{a}_0}{(\mathbf{a}_0^{-3} - 1)} \left[ D_+(z_d) + (1+z_d) \frac{dD_+(z_d)}{dz_d} \right]. \quad (18)$$

In Fig. 4 we have plotted  $\mathcal{S}(z_d) \div [-\delta_0 \log \mathbf{a}_0 / (\mathbf{a}_0^{-3} - 1)]$  for the top-hat cluster/void models of Eq. (13) to illustrate evolution of the structure parts of Eqs. (5) and (7). To obtain the  $z_d$  dependence of the structure part for a particular lens simply multiply each curve by the appropriate value of  $S_0 \equiv [-\delta_0 \log \mathbf{a}_0 / (\mathbf{a}_0^{-3} - 1)]$ . To understand why the various evolutionary schemes produce different central temperatures at  $z_d = 0$  for exactly the same perturbation density at  $z_d = 0$ , one has only to identify the two sources of the  $z_d$  dependence in Eq. (6). When the derivative acts on the  $(1+z_d)$  term the contribution to Eq. (4) is  $H_d T_p / (1+z_d)$  which is directly proportional to the potential part of the lensing time delay  $T_p$ . At the delayed exit, time the background CMB photons have further cooled and reddened whereas the lensed CMB photons, stuck in the lens, were not so reddened, and hence appear relatively bluer. This time-delay contribution to the temperature shift of the CMB is common to all evolutionary schemes and constitutes the entire temperature shift if the lens mass structure is evolving exactly like the background cosmology. If the lens density evolves differently than the background, transiting CMB photons can lose or gain energy by virtue of the changing depth of the transited gravitational potential within the Swiss cheese void. If the lens is more condensed in the past,  $\partial f(x, z_d) / \partial z_d > 0$  in Eq. (6), the fractional projected lens mass  $f(x, z_d)$  decreased with cosmic time and transiting photons lose less energy when

climbing out of the lens' potential well than they gain when falling in. They would thus appear even bluer because of the evolution. However, if  $\partial f(x, z_d)/\partial z_d < 0$ , the lens structure is becoming more condensed with time (as shown in Fig. 4 for linear perturbations) and the CMB photons are redshifted because of evolution. The larger the evolution rate the more reduction takes place in the time-delay blue shift. In the EdS universe  $D_+(z_d) \propto R(t_d)$  assuming linear evolution (see Eq. (18)), and the evolution reddening completely cancels the time-delay blue shift (see the solid red curve in Fig. 4). See Chen et al. [21] for more discussion about the time-delay and evolutionary contributions to the ISW effect.

## B. Virialized Clusters

The only relaxed cluster models (ones whose gravitational properties have ceased evolving with cosmic time) of the top-hat form given in Eq. (13) have  $\rho = 0$  in the compensation region,  $\mathbf{a} < x < 1$ , i.e.,

$$\delta = (\mathbf{a}^{-3} - 1) \quad \text{and} \quad \mathbf{a} = \mathbf{a}_0(1 + z_d). \quad (19)$$

This particular comoving evolution cancels the background cosmology's expansion leaving the cluster with a constant physical size and central mass density. We can parameterize these models by their current ( $z_d = 0$ ) density contrast  $\delta_0 = \rho_{\text{vir}}/\bar{\rho}_0 - 1$ , or by their current fractional radius  $\mathbf{a}_0 < 1$ , or by a “freeze” redshift  $z_f$  at which  $\mathbf{a} = 1$  (equivalently when  $\delta = 0$ ). These three parameters are related by  $\mathbf{a}_0 = (1 + \delta_0)^{-1/3} = (1 + z_f)^{-1}$ . The virialized cluster's density contrast  $\delta$  evolves with cosmic time and when written as a function of the cluster's redshift  $z_d$  is

$$1 + \delta(z_d) \equiv \frac{\rho_{\text{vir}}}{\bar{\rho}(z_d)} = \frac{1 + \delta_0}{(1 + z_d)^3}, \quad (20)$$

and has an evolving fractional comoving radius

$$\mathbf{a}(z_d) = \frac{1 + z_d}{(1 + \delta_0)^{1/3}}. \quad (21)$$

Eventhough these models can only represent virialized clusters after virialization at redshift  $z_v$ , they can be extended back to earlier redshifts  $z_f$  where  $\delta = 0$  and  $\mathbf{a} = 1$ . At that instant they would represent comoving spheres of the background cosmology that suddenly froze. After  $z_f$  the Universe would continue to expand leaving them forever as static spheres with their original densities and radii, surrounded by completely voided spherical wells that grow

in thickness with cosmic time. The form of the evolving structure function Eq. (15) for these top-hat cluster models is quite simple

$$\mathcal{S}(z_d) = -1 + \log \left[ \frac{(1 + \delta_0)^{1/3}}{1 + z_d} \right]. \quad (22)$$

An arbitrary set of structure curves from Eq. (22) are shown in Fig.5 and represent possible evolutionary trajectories for clusters once they have virialized. The actual curve for a given cluster depends on when it was virialized (i.e., at what redshift  $z_v$ ) and what density contrast  $\delta_v$  it had at virialization. If we rewrite Eq. (22) using these two parameters we have

$$\mathcal{S}(z_d) = -1 + \frac{1}{3} \log(1 + \delta_v) + \log \left[ \frac{1 + z_v}{1 + z_d} \right]. \quad (23)$$

We use the virialization theory of [46] to determine which structure curves  $\mathcal{S}(z_d)$  are possible for a given background cosmology. Accordingly, if virialization takes place at redshift  $z_v$  then its density contrast  $\delta_v$  at that redshift is given by

$$1 + \delta_v \equiv \frac{\rho_{\text{vir}}}{\bar{\rho}(z_v)} = \frac{\Delta_c(z_v)}{\Omega_m(z_v)}, \quad (24)$$

where the mass density parameter at  $z_v$  depends on the cosmology, e.g.,  $\Omega_m(z_v) = \Omega_m(1 + z_v)^3/E(z_v)^2$  and  $\Delta_c(z_v)$  is an approximated function of  $x \equiv \Omega_m(z_v) - 1$  which also depends on the background cosmology [46]

$$\Delta_c(z_v) \equiv \frac{\rho_{\text{vir}}}{\rho_{\text{crit}}(z_v)} = \begin{cases} 18\pi^2 + 60x - 32x^2, & \Omega_\Lambda = 0, \\ 18\pi^2 + 82x - 39x^2, & \Omega_m + \Omega_\Lambda = 1. \end{cases} \quad (25)$$

In Fig.5 we have plotted  $\mathcal{S}(z_d = z_v)$  of Eq. (23) with  $\delta_v(z_v)$  determined by Eq. (24) for the four cosmologies,  $(\Omega_m, \Omega_\Lambda) = (0.05, 0)$  cyan,  $(0.3, 0)$  blue,  $(1, 0)$  red, and  $(0.3, 0.7)$  green, respectively top to bottom. Any point on one of these curves represent a starting point for a cluster's structure function to begin its evolution. For example the black curve that starts at  $S(2.0) = 0.5$  and ends at  $S(0) = 1.6$  could represent a cluster evolving in any of the four cosmologies considered. It could have been virialized at  $z_v = 1.63$  in a  $(\Omega_m, \Omega_\Lambda) = (0.3, 0.7)$  cosmology, at  $z_v = 1.4$  in a  $(\Omega_m, \Omega_\Lambda) = (1, 0)$  cosmology, at  $z_v = 1.05$  in a  $(\Omega_m, \Omega_\Lambda) = (0.3, 0)$  cosmology, or at  $z_v = 0.15$  in a  $(\Omega_m, \Omega_\Lambda) = (0.05, 0)$  cosmology. After forming at any of these points a cluster's function  $\mathcal{S}(z_d)$  evolves upward and to the left on the  $\delta_0 = 2440$  curve, provided the cluster doesn't merge with any of its neighbors. Because most clusters are currently thought to be discovered near verilization, they would lie near the one of the

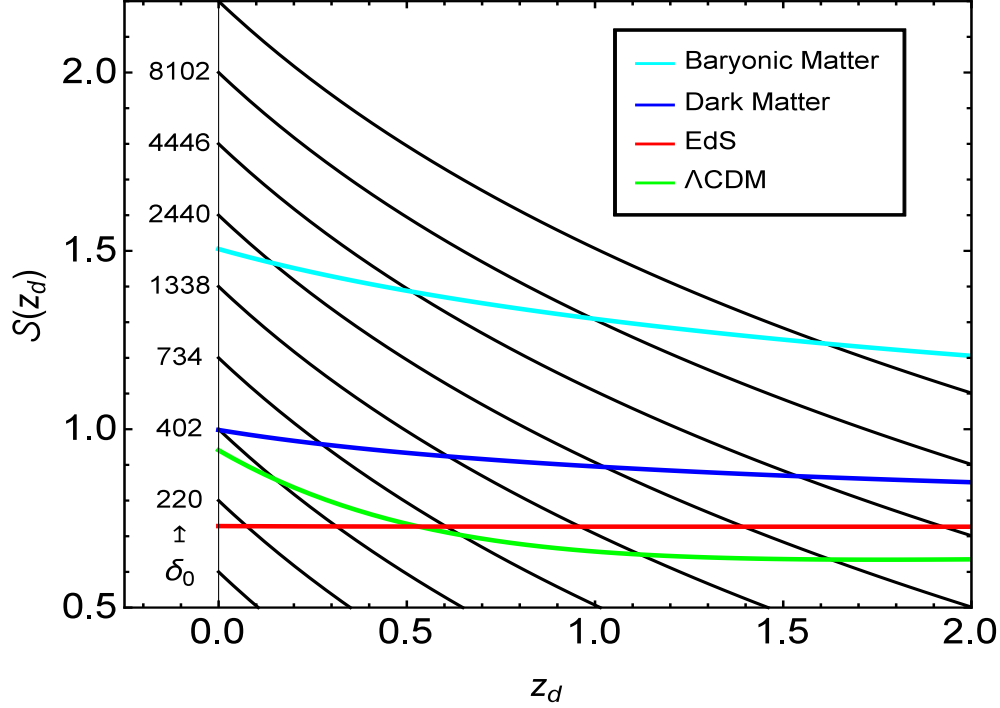


FIG. 5. Evolving structure functions  $\mathcal{S}(z_d)$  for virialized clusters (black curves). Each curve represents a fixed cluster as seen by observers at different redshifts  $z_d$  and is labeled on the left by,  $\delta_0$ , its excess central density fraction at  $z_d = 0$ . For a virialized cluster to actually exist in a given background cosmology it must be created at some redshift  $z_v$  with excess density  $\delta_v$ , see Eq. (24). The value of  $\mathcal{S}(z_d = z_v)$  at virialization is determined by Eq. (23). Once virialized the cluster then evolves up and to the left on the corresponding black curve. The four approximately horizontal curves (respectively top-down) are the starting points for clusters in a baryonic-matter only universe,  $(\Omega_m, \Omega_\Lambda) = (0.05, 0)$ , plotted in cyan; in a dark matter only universe,  $(\Omega_m, \Omega_\Lambda) = (0.3, 0)$ , plotted in blue; in the Einstein de Sitter universe,  $(\Omega_m, \Omega_\Lambda) = (1, 0)$ , plotted in red; and in a  $\Lambda$ CDM universe,  $(\Omega_m, \Omega_\Lambda) = (0.3, 0.7)$ , plotted in green.

creation lines. Perhaps the structure function for fossil groups would be more likely to follow the black curves. Given the masses and central densities of a set of clusters Fig. 5 ideally gives the  $\mathcal{S}(z_d)$  values of these clusters and Eq. (5) relates the CMB temperature increase caused by each cluster to the Hubble parameter at each cluster's redshift.

## IV. CONCLUSIONS

The ISW effect has been recently detected via the aperture photometry method (stacking/averaging patches of the CMB maps around known cosmic voids or galaxy clusters) by several groups [3, 5, 9, 10] and future observations promise more and better data. We present a new method of using this data to constrain the cosmological parameters by applying the ISW effect to individual inhomogeneities such as galaxy clusters and cosmic voids. We were able to develop this ISW-redshift test only after discovering a simple relation between the Fermat potential of an embedded lens and the frequency shift of photon crossing that lens. However, to use this test to extract the Hubble parameter and/or the curvature parameters the evolution of the lens has to be understood. We have illustrated the use of the ISW-z test by constructing models for clusters and voids with very simple density profiles and simple evolutions (i.e., top-hats for linearly evolving clusters/voids and completely virialized clusters). For cosmic voids, neither the density profile nor the time evolution is well constrained by observations. Consequently, the proposed ISW-z test might be more appropriately used to constrain the void's structure function  $\mathcal{S}(z_d)$ , e.g., the dark matter profile and its evolution, by assuming a specific cosmology (e.g.,  $\Lambda$ CDM) and using the CMB observations. There are several theoretical/numerical papers modeling the formation and evolution of cosmic voids [42–44, 47] which can be used to estimate the structure term  $\mathcal{S}(\theta_I, z_d)$  of Eq. (6) and the ISW-z test can possibly confirm or reject such models as more data becomes available. The density profile of galaxy clusters is much better constrained than cosmic voids, and for their low redshift evolution it is reasonable to assume that they are virialized. Consequently, the structure term  $\mathcal{S}(\theta_I, z_d)$  can in principle be accurately modeled. At this point, however, the CMB observations are contaminated by the foreground emission from the clusters and SZ effect. The modeling of the ISW effect caused by an embedded galaxy cluster with physical profiles such as NFW is the obvious next step.

- 
- [1] R. K. Sachs & A. M. Wolfe, *Astrophys. J.* **147**, 73 (1967).
  - [2] M. J. Rees & D. W. Sciama, *Nature* **217** 511 (1968).
  - [3] B. R. Granett, M. C. Neyrinck, & I. Szapudi, *Astrophys. J. Lett.* **683**, 99 (2008a).
  - [4] B. R. Granett, M. C. Neyrinck, & I. Szapudi, arXiv.0805.2974 (2008b).

- [5] Planck Collaboration, P. A. R. Ade, et al. *Astron. Astrophys.*, submitted, arXiv1303.5079 (2013).
- [6] K. T. Inoue & J. Silk, *Astrophys. J.* **648**, 23 (2006).
- [7] L. Rudnick, S. Brown, & L. R. Williams, *Astrophys. J.* **671**, 40 (2007).
- [8] S. Nadathur, S. Hotchkiss, & S. Sakar, *JCAP*, 06, 042 (2012).
- [9] C. Hernández-Monteagudo, *Astron. Astrophys.* 520, 101 (2010).
- [10] S. Ilić, M. Langer, & M. Douspis, *Astron. Astrophys.* 556, 51 (2013).
- [11] G. Lavaux & B. D. Wandelt, *Astrophys. J.* **754**, 109 (2012).
- [12] J-B. Melin & J. G. Bartlett, *Astron. Astrophys.*, submitted, astro-ph:1408.5633 (2014).
- [13] U. Chantavat, U. Sawangwit, P. M. Sutter, & B. D. Wandelt, astro-ph:1409.3364 (2014).
- [14] N. Hamaus, P. M. Sutter, G. Lavaux, & B. D. Wandelt, astro-ph:1409.3580 (2014).
- [15] J. H. Cooke & R. Kantowski, *Astrophys. J. Letters*, 195, 11 (1975).
- [16] R. Kantowski, B. Chen, and X. Dai, *Astrophys. J.* **718**, 913 (2010).
- [17] B. Chen, R. Kantowski, and X. Dai, *Phys. Rev. D* **82**, 043005 (2010).
- [18] B. Chen, R. Kantowski, and X. Dai, *Phys. Rev. D* **84**, 083004 (2011).
- [19] R. Kantowski, B. Chen, and X. Dai, *Phys. Rev. D* **86**, 043009 (2012).
- [20] R. Kantowski, B. Chen, and X. Dai, *Phys. Rev. D* **88**, 083001 (2013).
- [21] B. Chen, R. Kantowski, and X. Dai, *Astrophys. J.* submitted, arXiv1310.7574 (2013).
- [22] B. Chen, R. Kantowski, and X. Dai, *Astrophys. J.* submitted, arXiv1310.7574 (2013).
- [23] A. Einstein & E. G. Straus, *Rev. Mod. Phys.* **17**, 120 (1945).
- [24] E. Schücking, *Z. Phys.* **137**, 595 (1954).
- [25] R. Kantowski, *Astrophys. J.* 155, **89** (1969).
- [26] G. Lemaitre, *Ann. Soc. Bruxelles* **A53**, 51 (1933).
- [27] R. C. Tolman, *Proc. Natl. Acad. Sci.* **20**, 169 (1934).
- [28] H. Bondi, *Mon. Not. R. Astron. Soc.* **107**, 410 (1947).
- [29] L. Nottale, *Mon. Not. R. Astron. Soc.* **206**, 713 (1984).
- [30] E. Martínez-González, J. L. Sanz, & J. Silk, *Astrophys. J. Lett.* **355**, 5 (1990).
- [31] M. Panek, *Astrophys. J.* **388**, 225 (1992).
- [32] U. Seljak, *Astrophys. J.* **460**, 549 (1996).
- [33] N. Sakai & K. T. Inoue, *Phys. Rev. D* **78**, 063510 (2008).
- [34] W. Valkenburg, *JCAP* **06**, 010 (2009).



- [35] P. Schneider, J Ehlers, and E. E. Falco, *Gravitational Lenses* (Springer-Verlag, Berlin, 1992).
- [36] P. M. Sutter, G. Lavaux, B. D. Wandelt, & D. H. Weinberg, *Astrophys. J.* 761, 44 (2012).
- [37] K. N. Abazajian, J. K. Adelman-McCarthy, M. A. Agüeros, et al., *Astrophys. J. Suppl. Ser.* 182, 543 (2009).
- [38] P. M. Sutter, G. Lavaux, B. D. Wandelt, & D. H. Weinberg, M. S. Warren, *Mon. Not. R. Astron. Soc.* submitted, arXiv1311.3301 (2013).
- [39] J. F. Navarro, C. S. Frenk, & S. D. White, *Astrophys. J.* 462, 563 (1996).
- [40] R. A. Sunyaev & Y. B. Zeldovich, *Mon. Not. R. Astron. Soc.* 190, 413 (1980).
- [41] M. Birkinshaw, *Phys. Rep.* 310, 97 (1999).
- [42] J. P. Ostriker & L. L. Cowie, *Astrophys. J. Lett.* 243, 127 (1981).
- [43] E. Bertschinger, *Astrophys. J. Suppl. Ser.* 58, 1 (1985a).
- [44] E. Bertschinger, *Astrophys. J. Suppl. Ser.* 58, 39 (1985b).
- [45] D. J. Heath, *Mon. Not. R. Astron. Soc.* 179, 351 (1977).
- [46] G. L. Bryan & M. L. Norman, *Astrophys. J.* 495, 80 (1998).
- [47] R. K. Sheth & R. van de Weygaert, *Mon. Not. R. Astron. Soc.* 350, 517 (2004).